High-resolution lung MRI with Ultrashort-TE: 1.5 or 3 Tesla?

Guillaume Chassagnon, Charlotte Martin, Wadie Ben Hassen, Gael Freche, Souhail Bennani, Baptiste Morel, Marie-Pierre Revel

High-resolution lung MRI with Ultrashort-TE: 1.5 or 3 Tesla?

Guillaume CHASSAGNON, M.D. (1) (2) ; Charlotte MARTIN, M.D. (1) ; Wadie BEN HASSEN, Ph.D. (3) ; Gael FRECHE, M.D. (1) ; Souhail BENNANI, M.D. (1) ; Baptiste MOREL, M.D. PhD (4) ; Marie-Pierre REVEL, M.D. Ph.D. (1)

Institutions:

(1) Radiology Department, Groupe Hospitalier Cochin-Hotel Dieu, AP-HP, Université Paris Descartes, 27 Rue du Faubourg Saint-Jacques, 75014 Paris, France

(2) Center for Visual Computing, Ecole CentraleSupelec, 3 Rue Joliot Curie, 91190, Gif-sur-Yvette, France

(3) Siemens Healthineers France, 40 avenue des fruitiers, 93210 Saint-Denis, France

(4) Radiology Department, Hopital Clocheville, CHU Tours, Université François Rabelais, 49 Boulevard Béranger, 37000 Tours, France

Corresponding author:

Marie-Pierre REVEL

Address: Service de Radiologie A, Groupe Hospitalier Cochin Broca Hôtel-Dieu, AP-HP, 27 Rue du Faubourg Saint-Jacques, 75014 Paris, France

Phone: 00-33-1-42-34-79-10 / Fax: 00-33-1-43-26-65-52

Email: marie-pierre.revel@aphp.fr

Acknowledgements:

The authors would like to thank Alto Stemmer, Thomas Benkert, and Josef Pfeuffer from Siemens Healthineer for providing the UTE spiral VIBE sequence and the SPIRiT reconstruction.

Funding: This study was sponsored by Assistance Publique – Hôpitaux de Paris (Département de la Recherche Clinique et du Développement)

1. INTRODUCTION

Lung magnetic resonance imaging (MRI) is an evolving field, and MRI may be increasingly used to evaluate chronic lung diseases in the near future [1]. The functional results of recent techniques such as T1 mapping and Fourier decomposition have been found to be promising in the lungs, especially for cystic fibrosis and chronic obstructive pulmonary disease assessment [2–6]. Recently, high-resolution lung MRI has been made possible by the development of ultrashort echo time (UTE) sequences using non-cartesian k-space sampling and respiratory gating to compensate for respiratory motion. These sequences compensate for the low proton density and very short transverse relaxation time (T2*) of the lung parenchyma [7–11].

Several high-resolution lung MRI sequences with near-millimeter resolution have been reported, with different image qualities [7–11]. Most of them use radial sampling of the k-space and a navigator for respiratory gating. The PETRA sequence has been reported to allow visualization of the distal bronchi at 1.5T [9] with good agreement with computed tomography for morphological scoring of bronchial disease in cystic fibrosis patients [12].

High-resolution lung MRI sequences have been reported at both 1.5 and 3T magnetic fields. According to Lederlin and Crémillieux, there is a theoretical advantage of 3T because the signal-to-noise ratio should be higher [13]. However, this theoretical advantage might be counterbalanced by the increase of the magnetic susceptibility effects within lung parenchyma and subsequent shortening of T2* relaxation time. To the best of our knowledge, there have been no reports comparing the same high-resolution lung MRI sequence at 1.5 and 3T magnetic field. Therefore, the exact influence of magnetic field strength on image quality of the lung is not known and should be evaluated.

Optimizing high resolution lung MRI protocols is complex and is not only based on the choice of magnetic field. Indeed, there are several other parameters influencing both image

quality and acquisition/reconstruction times such as spatial resolution, the setting of the non-Cartesian sampling used to accelerate k-space filling, and the optional use of an iterative reconstruction technique to accommodate for under-sampling of the k-space.

A prototype free-breathing UTE technique based on 3D-GRE sequence with volumetric interpolation (VIBE) sequence and spiral sampling to cover the k-space was recently developed [14]. This sequence can be performed at both 1.5 and 3T and uses prospective intrinsic gating to obtain near-millimeter high-resolution lung MR images during free-breathing.

The purpose of this study was to assess the influence of magnetic field strength and additionally of acquisition and reconstruction parameters on the quality of high-resolution lung MRI, using a prototypical UTE sequence.

2. MATERIALS AND METHODS

This study was approved by a national ethics committee (Blinded for review). All participants provided written informed consent prior to examination. One investigator (Blinded for review) was an employee of Siemens Healthineers but did not participate in the evaluation of image quality. The remaining authors had full control of the data presented in this article.

2.1. Study Population

From January to February 2018, 10 healthy volunteers were included (6 men and 4 women [mean age ±standard deviation (SD)= 26.8 ±3.7 and 27.9 ±2.4, respectively; p=0.933]). They had no history of smoking, no respiratory symptoms or history of lung disease. Mean height and weight ±SD were 176 ±9cm and 69.2 ±10.5kg, respectively. All images were anonymized for evaluation.

2.2. Image Acquisition

MR images were acquired on 1.5 Tesla (MAGNETOM Aera, Siemens Healthineers, Erlangen, Germany) and 3 Tesla (MAGNETOM Skyra, Siemens Healthineers) units on the same day, using a prototype UTE spiral VIBE sequence [14]. The two MR scanners had similar gradient performances and the same software version (syngo MR VE11).

The characteristics of the sequence are as follows: k-space data are acquired following a stack-of-spirals scheme where Cartesian phase encoding is used for slice encoding. Spiral sampling is performed for in-plane encoding. To minimize echo time, each spiral readout starts directly after the 3D phase encoding gradient [15] and non-selective RF pulses are used. The free-breathing sequence uses intrinsic prospective respiratory gating, with real time evaluation of breathing during scanning. When sufficient data have been acquired, the sequence acquisition automatically stops and images are reconstructed. The expiratory phase is used for gating, since its duration is typically longer than the inspiratory phase and therefore, more data are available.

All images were acquired on the coronal plane, using an 18-channel body array combined with a 32-channel spine array on both MRI units. There were 20 active coil elements for each acquisition. Acquisitions were performed with the arms alongside the body. For evaluating the influence of magnetic field strength, acquisitions were performed with the following default acquisition parameters on each unit: TE 0.05ms, $1.2mm^3$ resolution, 464 spiral interleaves, in-plane acceleration parameter (iPAT factor) of 2, and iterative self-consistent parallel imaging reconstruction (SPIRiT) reconstruction (Table 1). For evaluating the influence of other parameters, 3 additional sequences were acquired, with only one change in acquisition or reconstruction parameter for each sequence, compared to the default setting:

- At 1.5 Tesla, one acquisition with Non-Uniform Fourier Transform (NUFFT) reconstruction instead of SPIRiT reconstruction, and another with a decreased number

of spiral interleaves (264 instead of 464)

- At 3 Tesla, one acquisition with 1.0mm^3 resolution

Thus, 5 acquisitions were performed for each volunteer. Each spiral readout lasted 1800 µs at 1.5T and 1160 µs at 3T to compensate for the shorter T2* at 3T. These values were those recommended by the manufacturer. Acquisition and reconstruction times were recorded. The objective when performing these 5 acquisitions was to assess the effects of magnetic field strength, voxel resolution, number of spiral interleaves and reconstruction algorithm on image quality and examination time. Comparisons were performed between 2 sequences having only one difference in acquisition or reconstruction parameter.

2.3. Visual Assessment of Image Quality

Signal homogeneity, visibility of fissures and the presence of artifacts were subjectively assessed by two radiologists with 1 and 3-years experience in thoracic imaging (Blinded for review). Signal homogeneity was rated as 0=poor, 1=fair, 2=good, or 3=very good. Visibility of vertical and horizontal fissures was rated as 0=not visible, 1=visibility<50%, 2=visibility>50%, or 3=complete visibility. The average visibility score of the three fissures was calculated for each sequence. Artifacts (ringing and streaking) were rated as 0=absent, 1=mild, 2=moderate, or 3=severe. The proportion of visible airways from the trachea (generation 0) down to the subsegmental level (generation 4) was analyzed using the Boyden classification [16]. This proportion was calculated for a total of 68 airways on 5 sequences in 10 patients, thus for a total of 3400 bronchi.

2.4. Objective Assessment of Image Quality

Measurement of signal intensity was adapted from the method proposed by Dournes et al [9]. Briefly, 30mm^2 regions of interest (ROI) were drawn on images reformatted in the axial plane. Signal intensity of the lung parenchyma was measured by drawing ROIs in the anterior and posterior areas of each lung, at a distance of at least 20 mm from the pleura and not including visible pulmonary vessels. These ROIs were drawn at 3 different levels: 1/ the aortic arch, 2/ the carina, and 3/ the right pulmonary inferior vein. Signal intensity in the airways was measured by drawing ROIs in the lumen of the trachea, the intermediate bronchus and the left main bronchus at the level of the left upper lobe bronchus. Signal intensity of the vessels was measured in the pulmonary trunk and in the right and left main pulmonary arteries. The average signal intensity (SI) was calculated from 12 ROIs for the lung parenchyma (SI_{lung}) and 3 ROIs for both the airways ($SI_{airways}$) and the pulmonary vessels ($SI_{vessels}$). Signal-to-noise (SNR) and contrast-to-noise (CNR) ratios were calculated as follows: $SNR = (SI_{lung} / SI_{airway}) \cdot 100\%$, and $CNR = (SI_{lung} - SI_{airway}) / SI_{vessel} \cdot 100\%$. Signal measurements were performed by 2 radiologists (Blinded for review), with 3- and 1-year experience in thoracic imaging, respectively, in order to assess interobserver repeatability.

2.5. Statistical Analysis

Statistical analysis was performed using 'R' software (version 3.3.3, R Foundation, Vienna, Austria). Continuous variables are presented as means ±SD. Agreement between observers was evaluated using the McNemar test for airways visibility. Interobserver repeatability for SNR and CNR measurements was evaluated using Intraclass Correlation Coefficients. Interobserver agreement for the rating of fissure visibility, signal homogeneity and artifacts was evaluated using weighted (squared) kappa test. For further analysis, measurements from the 2 observers were combined. In order to separately analyze the influence of each parameter (magnetic field strength, voxel size, number of spiral interleaves, and iterative or non-iterative

reconstruction mode), comparison of SNR, CNR, airways and fissure visibility, signal homogeneity and artifacts was performed between sequences with only one different acquisition or reconstruction parameter, using a paired t test. A *P* value <0.05 was considered to be statistically significant.

3. RESULTS

3.1. Visual Assessment of Image Quality

There was no significant difference between the 2 observers for the proportion of visible airways (p=0.120). There was also a good inter observer agreement for the rating of fissure visibility (kappa = 0.71; p<0.001), the presence of ringing (0.80; p<0.001) and streaking (kappa = 0.77; p<0.001) artifacts and perfect agreement for the rating of signal homogeneity (kappa = 1; p<0.001). All lobar bronchi and nearly all segmental bronchi were visible (94 ±16 to 99 ±3 % depending on the acquisition and reconstruction parameters) (Table 2) whereas only 35 ±18 to 73 ±14% of the subsegmental bronchi were depicted (figure 1).

Visibility of the subsegmental bronchi and fissures was significantly decreased at 3T (p<0.001 for both) (figure 2), and ringing artifacts were increased (p<0.001). Reducing the number of spiral interleaves similarly decreased the visibility of the subsegmental bronchi and fissures (p<0.001 for both) and increased ringing artifacts (p=0.028). Using the non-iterative reconstruction mode (NUFFT reconstruction) rather than the SPIRiT algorithm also decreased the visibility of the subsegmental bronchi (p<0.001) and fissure (p=0.003) and increased ringing artifacts (p=0.049). Conversely, the visibility of the subsegmental bronchi was significantly improved with higher resolution (1.0mm^3 vs 1.2 mm^3, p=0.001), even though visibility with 1.0mm^3 resolution at 3T was less than at 1.5T with 1.2mm^3 resolution (p<0.001). Sequences with 1.0mm^3 resolution could not be acquired at 1.5T.

Signal homogeneity was rated as very good (3/3) for almost all acquisitions (50/50 for observer 1 and 49/50 for observer 2). A significant increase of streaking artifacts ($p<0.001$) was observed with the NUFFT reconstruction mode (figure 3) due to k-space undersampling.

3.2. Objective Assessment of Image Quality

Intraclass correlation coefficients for repeatability of SNR and CNR measurements were 0.92 and 0.89 respectively. Although the signal intensity of the lung parenchyma was 1.4-fold higher at 3T than at 1.5T with the default parameters (99.4 ±22.3 vs 70.7 ±12.3, $p<0.001$), SNR and CNR were significantly lower (140.2 ±19.9 vs 190.2 ±34.8, $p=<0.001$; and 5.7 ±2.4 vs 10.8 ±2.8, $p<0.001$, respectively). The use of fewer spiral interleaves ($p= 0.09$) or a higher resolution ($p=0.018$) also resulted in a significant decrease in SNR. SNR and CNR were not significantly influenced by the use of NUFFT reconstruction ($p=0.364$ and $p=0.548$, respectively).

3.3. Acquisition and Reconstruction Times

The mean acquisition and reconstruction times ranged from 4.9 ±0.5 to 8.7 ±0.8 minutes, and from 1.7 ±0.2 to 17 ±3.0 minutes, respectively (Table 2). Acquisition time was significantly longer when the resolution was increased ($p=0.015$) and shorter when the number of spiral interleaves was decreased ($p<0.001$). Reconstruction time was significantly shorter with NUFFT than with SPIRiT ($p<0.001$). Reconstruction time at 3T was significantly longer due to less power of the calculator on the 3T unit ($p<0.001$).

4. DISCUSSION

To the best of our knowledge, this study is the first to compare 1.5 and 3T magnetic fields for high-resolution lung MRI using UTE sequences. Nearly all bronchi were visible up to the

segmental level at both 1.5 and 3T magnetic fields in healthy volunteers. SNR and CNR were lower at 3T with a decreased visibility of the fissures and subsegmental bronchi, and an increase of ringing artifacts. Decreasing the number of spiral interleaves and using non-iterative reconstruction also negatively influenced the image quality, whereas higher resolution improved the visibility of the subsegmental bronchi.

Despite the reduced T2* relaxation time at 3T (2.1 vs 0.74ms) [17], several authors suggested that 3T acquisitions would represent a significant advantage for lung parenchyma imaging because of the 2-fold gain in proton signal [13,18]. Even though Gai et al predicted a 1.8-fold increase in SNR [18] and we observed a 1.4-fold increase in the lung parenchyma signal at 3T, the increase in noise and artifacts resulted in a significantly lower SNR compared to 1.5T. The decrease of transverse relaxation time was faster than anticipated at 3T, resulting in less signal at the end of the spiral readout, despite reducing the readout window from 1800 µs at 1.5T to 1160µs. Visually assessed image quality at 1.5T was also higher. Whereas signal homogeneity was very good on 3T images, ringing artifacts were also significantly increased. Evaluating a non-UTE VIBE sequence, Fink et al also reported lung MRI quality at 1.5 T to be higher than at 3 T, despite a higher contrast at 3T [19]. Dynamic 2 D lung MRI sequences have also been compared at different magnetic field strength. At 3 T, GRE sequences were the best option, whereas at 1.5 T, SSFP with an acceleration factor of 2 was considered the best compromise of temporal and spatial resolution [20].

In digital imaging, spatial resolution is defined as the ability to distinguish 2 separate structures and should not be confused with voxel size or matrix resolution. In experimental studies, spatial resolution can be quantified with the point spread function [21]. In previous reports of high-resolution lung MRI, all with near-millimeter voxel size, the spatial resolution on the provided images seemed highly heterogeneous [7–11].

A compromise between a high matrix resolution and SNR is important for MRI sequence optimization [22]. When voxel size is decreased, the amount of signal received by each individual voxel of the matrix is reduced. A significant decrease in SNR may induce a loss in spatial resolution. Kale et al have shown that human readers are more willing to lose fine details in the image for greater SNR [22]. In our study, decreasing the voxel size from 1.2 to 1.0mm^3 at 3T resulted in an increased visibility of the subsegmental bronchi without a significant decrease in SNR. Even though higher resolution could be obtained at 3T without significantly decreasing SNR, there was less signal and more artifacts resulting in lower quality scores as compared with 1.5T.

In MRI, while image contrast mostly depends on the low frequencies in the center of the k-space, image sharpness is contained in the high frequencies located at the periphery. For lung MRI, the use of radial or spiral sampling of the k-space to compensate for respiratory motion and the very short T2*, results in undersampling of the peripheral k-space and thus, blurrier images. Undersampling of the peripheral k-space tends to be more significant with spiral acquisitions due to longer data collection and off-resonance induced signal decay [15,23]. Blurring artifacts can be limited by increasing the number of spiral interleaves. The optimal number of spiral interleaves should be a compromise between acquisition time and tolerable blurring. We found that decreasing the number of spiral interleaves from 464 to 264 significantly decreased image quality, even though the advantage was to reduce the mean acquisition time by 3 minutes. Even though we think that the improved image quality is worth the extra acquisition time, the clinical relevance of such improvement remains to be clinically validated.

The final parameter evaluated in our study was iterative reconstruction. Compared to Cartesian k-space sampling, the non-Cartesian strategy requires more sophisticated reconstruction methods such as non-uniform fast Fourier transform (NUFFT) or SPIRiT [23].

NUFFT is a conventional reconstruction method using a gridding approach that can be adapted to reconstruct spiral MRI [24,25]. SPIRiT is a recent iterative reconstruction algorithm designed to reconstruct from arbitrary k-space sampling [26]. However, iterative reconstruction algorithms are usually more computationally demanding than direct reconstruction methods, such as NUFFT [26]. In our study, SPIRiT reconstruction significantly reduced streaking artifacts, known to be more pronounced with gridding algorithms than with iterative reconstruction [27]. This is expected, since undersampling combined with a regular NUFFT reconstruction results in these artifacts. However, the use of SPIRiT also resulted in a 370% increase in mean reconstruction time.

This study has several limitations. First, the UTE spiral VIBE sequence was not compared to other high-resolution lung MRI sequence such as PETRA. However, this comparison was not possible because PETRA is no longer supported in the latest MAGNETOM units. Moreover, PETRA results have only been reported at 1.5 T. A second potential limitation is that we only evaluated healthy volunteers and not diseased patients. Johnson et al. hypothesized that 1.5T images could improve the evaluation of lung diseases with increases in soft tissue or fluid, due to the longer T2* at this magnetic field [7]. Another limitation was the use of slightly different acquisition parameters at 3 T and 1.5 T. A different field-of-view was used for 1.5T and 3T because these were the optimized protocols for each MR unit and they were not changed for the present study.

In conclusion, we have shown that high-resolution lung MRI using UTE spiral VIBE sequence is feasible at both 1.5 and 3T. Better bronchi visualization, SNR and CNR, as well as less ringing artifacts were observed at 1.5T. In addition, decreasing the number of spiral interleaves and using non-iterative reconstruction negatively influenced the image quality, whereas higher resolution improved the detectability of the subsegmental bronchi but resulted in longer acquisition time. The clinical relevance of these changes needs to be confirmed by

further research.

REFERENCES

[1] Wielpütz MO, Mall MA. Imaging modalities in cystic fibrosis: emerging role of MRI. Curr Opin Pulm Med 2015;21:609–16. doi:10.1097/MCP.0000000000000213.

[2] Bauman G, Puderbach M, Heimann T, Kopp-Schneider A, Fritzsching E, Mall MA, et al. Validation of Fourier decomposition MRI with dynamic contrast-enhanced MRI using visual and automated scoring of pulmonary perfusion in young cystic fibrosis patients. Eur J Radiol 2013;82:2371–7. doi:10.1016/j.ejrad.2013.08.018.

[3] Dasenbrook EC, Lu L, Donnola S, Weaver DE, Gulani V, Jakob PM, et al. Normalized T1 magnetic resonance imaging for assessment of regional lung function in adult cystic fibrosis patients--a cross-sectional study. PloS One 2013;8:e73286. doi:10.1371/journal.pone.0073286.

[4] Jobst BJ, Triphan SMF, Sedlaczek O, Anjorin A, Kauczor HU, Biederer J, et al. Functional lung MRI in chronic obstructive pulmonary disease: comparison of T1 mapping, oxygen-enhanced T1 mapping and dynamic contrast enhanced perfusion. PloS One 2015;10:e0121520. doi:10.1371/journal.pone.0121520.

[5] Voskrebenzev A, Gutberlet M, Klimeš F, Kaireit TF, Schönfeld C, Rotärmel A, et al. Feasibility of quantitative regional ventilation and perfusion mapping with phase-resolved functional lung (PREFUL) MRI in healthy volunteers and COPD, CTEPH, and CF patients. Magn Reson Med 2017. doi:10.1002/mrm.26893.

[6] Kaireit TF, Gutberlet M, Voskrebenzev A, Freise J, Welte T, Hohlfeld JM, et al. Comparison of quantitative regional ventilation-weighted fourier decomposition MRI with dynamic fluorinated gas washout MRI and lung function testing in COPD patients. J Magn Reson Imaging JMRI 2017. doi:10.1002/jmri.25902.

[7] Johnson KM, Fain SB, Schiebler ML, Nagle S. Optimized 3D ultrashort echo time pulmonary MRI. Magn Reson Med 2013;70:1241–50. doi:10.1002/mrm.24570.

[8] Ohno Y, Koyama H, Yoshikawa T, Seki S. State-of-the-Art Imaging of the Lung for Connective Tissue Disease (CTD). Curr Rheumatol Rep 2015;17:69. doi:10.1007/s11926-015-0546-8.

[9] Dournes G, Grodzki D, Macey J, Girodet P-O, Fayon M, Chateil J-F, et al. Quiet Submillimeter MR Imaging of the Lung Is Feasible with a PETRA Sequence at 1.5 T. Radiology 2015;276:258–65. doi:10.1148/radiol.15141655.

[10] Roach DJ, Crémillieux Y, Serai SD, Thomen RP, Wang H, Zou Y, et al. Morphological and quantitative evaluation of emphysema in chronic obstructive pulmonary disease patients: A comparative study of MRI with CT. J Magn Reson Imaging JMRI 2016. doi:10.1002/jmri.25309.

[11] Delacoste J, Chaptinel J, Beigelman-Aubry C, Piccini D, Sauty A, Stuber M. A double echo ultra short echo time (UTE) acquisition for respiratory motion-suppressed high resolution imaging of the lung. Magn Reson Med 2017. doi:10.1002/mrm.26891.

[12] Dournes G, Menut F, Macey J, Fayon M, Chateil J-F, Salel M, et al. Lung morphology assessment of cystic fibrosis using MRI with ultra-short echo time at submillimeter spatial resolution. Eur Radiol 2016;26:3811–20. doi:10.1007/s00330-016-4218-5.

[13] Lederlin M, Crémillieux Y. Three-dimensional assessment of lung tissue density using a clinical ultrashort echo time at 3 tesla: a feasibility study in healthy subjects. J Magn Reson Imaging JMRI 2014;40:839–47. doi:10.1002/jmri.24429.

[14] Mugler JP, Fielden SW, Meyer CH, Altes TA, Miller GW, Stemmer A, et al. Breath-hold UTE Lung Imaging using a Stack-of-Spirals Acquisition, 23rd Annual Meeting of ISMRM, Toronto, Canada: 2015.

[15] Qian Y, Boada FE. Acquisition-weighted stack of spirals for fast high-resolution three-dimensional ultra-short echo time MR imaging. Magn Reson Med 2008;60:135–45. doi:10.1002/mrm.21620.

[16] Boyden EA. Segmental anatomy of the lungs. New York, NY: McGraw-Hill; 1955.

[17] Yu J, Xue Y, Song HK. Comparison of lung T2* during free-breathing at 1.5 T and 3.0 T with ultrashort echo time imaging. Magn Reson Med 2011;66:248–54. doi:10.1002/mrm.22829.

[18] Gai ND, Malayeri A, Agarwal H, Evers R, Bluemke D. Evaluation of optimized breath-hold and free-breathing 3D ultrashort echo time contrast agent-free MRI of the human lung. J Magn Reson Imaging JMRI 2016;43:1230–8. doi:10.1002/jmri.25073.

[19] Fink C, Puderbach M, Biederer J, Fabel M, Dietrich O, Kauczor H-U, et al. Lung MRI at 1.5 and 3 Tesla: observer preference study and lesion contrast using five different pulse sequences. Invest Radiol 2007;42:377–83. doi:10.1097/01.rli.0000261926.86278.96.

[20] Fabel M, Wintersperger BJ, Dietrich O, Eichinger M, Fink C, Puderbach M, et al. MRI of respiratory dynamics with 2D steady-state free-precession and 2D gradient echo sequences at 1.5 and 3 Tesla: an observer preference study. Eur Radiol 2009;19:391–9. doi:10.1007/s00330-008-1148-x.

[21] Li K, Garrett J, Ge Y, Chen G-H. Statistical model based iterative reconstruction (MBIR) in clinical CT systems. Part II. Experimental assessment of spatial resolution performance: Quantitative assessment of spatial resolution of MBIR method. Med Phys 2014;41:071911. doi:10.1118/1.4884038.

[22] Kale SC, Chen XJ, Henkelman RM. Trading off SNR and resolution in MR images. NMR Biomed 2009;22:488–94. doi:10.1002/nbm.1359.

[23] Tolouee A, Alirezaie J, Babyn P. Compressed sensing reconstruction of cardiac cine MRI using golden angle spiral trajectories. J Magn Reson 2015;260:10–9. doi:10.1016/j.jmr.2015.09.003.

[24] Sha L, Guo H, Song AW. An improved gridding method for spiral MRI using

nonuniform fast Fourier transform. J Magn Reson 2003;162:250–8.

[25] Fessler JA. On NUFFT-based gridding for non-Cartesian MRI. J Magn Reson 1997 2007;188:191–5. doi:10.1016/j.jmr.2007.06.012.

[26] Lustig M, Pauly JM. SPIRiT: Iterative self-consistent parallel imaging reconstruction from arbitrary k-space. Magn Reson Med 2010;64:457–71. doi:10.1002/mrm.22428.

[27] Uecker M, Zhang S, Frahm J. Nonlinear inverse reconstruction for real-time MRI of the human heart using undersampled radial FLASH. Magn Reson Med 2010;63:1456–62. doi:10.1002/mrm.22453.

Tables

Table 1. Acquisition parameters

	Default 1.5T	1.5T with 264 spiral interleaves	1.5T with NUFFT	Default 3T	3T with 1.0mm^3 resolution
Magnetic field	1.5T	1.5T	1.5T	**3T**	**3T**
Resolution (mm3)	1.2	1.2	1.2	1.2	**1.0**
Field of view (mm)	540	540	540	467	467
Echo Time (ms)	0.05	0.05	0.05	0.05	0.05
Repetition Time (ms)	4.19	4.19	4.19	4,07	4,07
Readout time (µs)	1800	1800	1800	1160	1160
Flip angle (°)	5	5	5	5	5
Number of spiral interleaves	464	**264**	464	464	464
iPAT Factor	2	2	2	2	2
Reconstruction mode	SPIRiT	SPIRiT	**NUFFT**	SPIRiT	SPIRiT

Difference with default sequences are highlighted in bold.

The number of slices was set according to patient's morphology

Abbreviations: NUFFT = Non-Uniform Fourier Transform, SPIRiT = iterative self-consistent parallel imaging reconstruction

Table 2. Comparison of examination time and image quality between the 5 acquired sequences

	Default 1.5T	1.5T with 264 spiral interleaves *(p value)**	1.5T with NUFFT *(p value)**	Default 3T (*p value*)*	3T with 1.0mm^3 resolution (*p value*) **
Acquisition time (min)	8.1 ±0.5	4.9 ±0.5 **(p<0.001)**	8.1 ±0.4 (p=0.815)	7.7 ±0.9 (p=0.101)	8.7 ±0.8 **(p=0.015)**
Reconstruction time (min)	8.0 ±0.5	9.0 ± 2.2 (p=0.177)	1.7 ±0.2 (p<0.001)	15.2 ±1.5 (p<0.001)	17.0 ±3.0 (p=0.094)
Visibility of bronchi (%)					
- Generation 0	100 ±0	100 ±0 (p>0.99)	100 ±0 (p>0.99)	100 ±0 (p>0.99)	100 ±0 (p>0.99)
- Generation 1	100 ±0	100 ±0 (p>0.99)	100 ±0 (p>0.99)	100 ±0 (p>0.99)	100 ±0 (p>0.99)
- Generation 2	100 ±0	100 ±0 (p>0.99)	100 ±0 (p>0.99)	100 ±0 (p>0.99)	100 ±0 (p>0.99)
- Generation 3	99 ±4	99 ±3 (p>0.99)	97 ±9 (p=0.167)	94 ±16 (p=0.098)	98 ±7 (p=0.144)
- Generation 4	73 ±14	46 ±17 **(p<0.001)**	57 ±18 **(p<0.001)**	35 ±18 **(p<0.001)**	45 ±17 **(p=0.001)**
Visibility of fissures (/3)	1.5 ±0.5	0.7 ±0.4 **(p<0.001)**	1.1 ±0.5 **(p=0.003)**	0.9 ±0.5 **(p<0.001)**	1.0 ±0.5 (p=0.681)
Signal homogeneity (/3)	3.0 ±0.0	3.0 ±0.0 (p>0.99)	3.0 ±0.0 (p>0.99)	2.9 ±0.2 (p=0.330)	3.0 ±0.0 (p=0.330)
Ringing artifacts (/3)	0.6 ±0.6	1.0 ±0.6 **(p=0.028)**	1.0 ±0.6 **(p=0.049)**	1.7 ±0.7 **(p<0.001)**	1.4 ±0.6 (p=0.149)
Streaking artifacts (/3)	0.0 ±0.0	0.1 ± 0.3 (p=0.163)	1.0 ±0.8 **(p<0.001)**	0.1 ±0.3 (p=0.162)	0.3 ±0.6 (p=0.186)
Signal to noise ratio (%)	190.2 ±34.8	165.8 ±20.5 **(p=0.009)**	185.9 ±28.5 (p=0.364)	140.2 ±19.9 **(p<0.001)**	131.3 ±9.9 (p=0.018)
Contrast to noise ratio (%)	10.8 ±2.8	9.8 ±2.1 (p=0.171)	10.6 ±2.6 (p=0.548)	5.7 ±2.4 **(p<0.001)**	5.2 ±1.6 (p=0.183)

Significant p values (< 0.05) are highlighted in bold.

* Comparison to the standard 1.5T acquisition

** Comparison to the standard 3T acquisition

Abbreviation: NUFFT = Non-Uniform Fourier Transform

Figure Legends

Figure 1. Subsegmental bronchi visualization depending on acquisition and reconstruction parameters. Subsegmental bronchi are visualized on the default protocol image at 1.5T (A), B1a (arrow) and B1b (arrowhead). With fewer spiral interleaves (B) or Non-Uniform Fourier Transform (NUFFT) reconstruction (C), B1a bronchus visibility is decreased and the B1b bronchus is no longer visible. Findings are similar on the default 3T protocol (D) and the 3T acquisition with 1.0 mm^3 resolution (E). With the default protocol at 3T (D), ringing artifacts (repetition lines) are mostly seen in the upper right part of the image (arrowhead).

Figure 2. Fissure visibility on default acquisitions at 1.5 and 3T. More than 50% of the left vertical fissure is seen at 1.5T (A), whereas less than 50% is seen at 3T.

Figure 3. Streaking artifact. Streaking artifact is seen in the lung parenchyma on images reconstructed with Non-Uniform Fourier Transform (NUFFT) (arrows in A and B). In the same patient, streaking artifacts are reduced on the default 1.5T acquisition reconstructed with iterative self-consistent parallel imaging reconstruction (SPIRiT) (C and D) and do not project in the lung parenchyma.

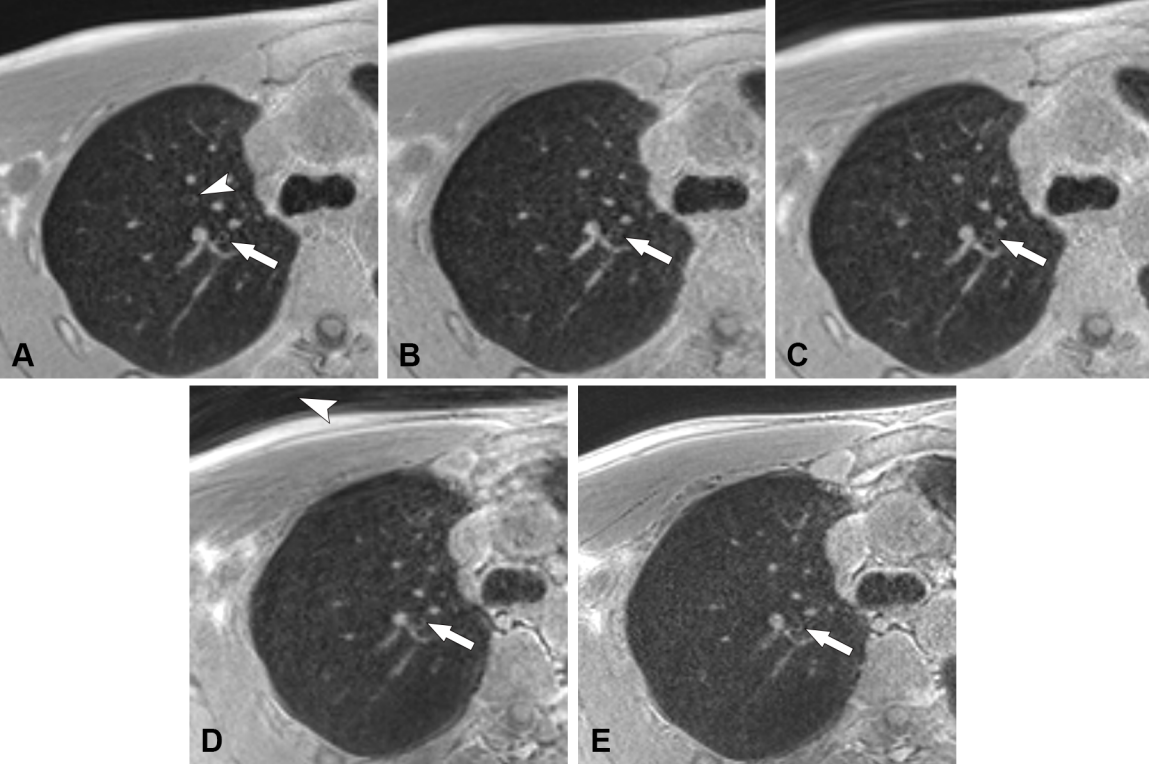
A
B
C
D
E

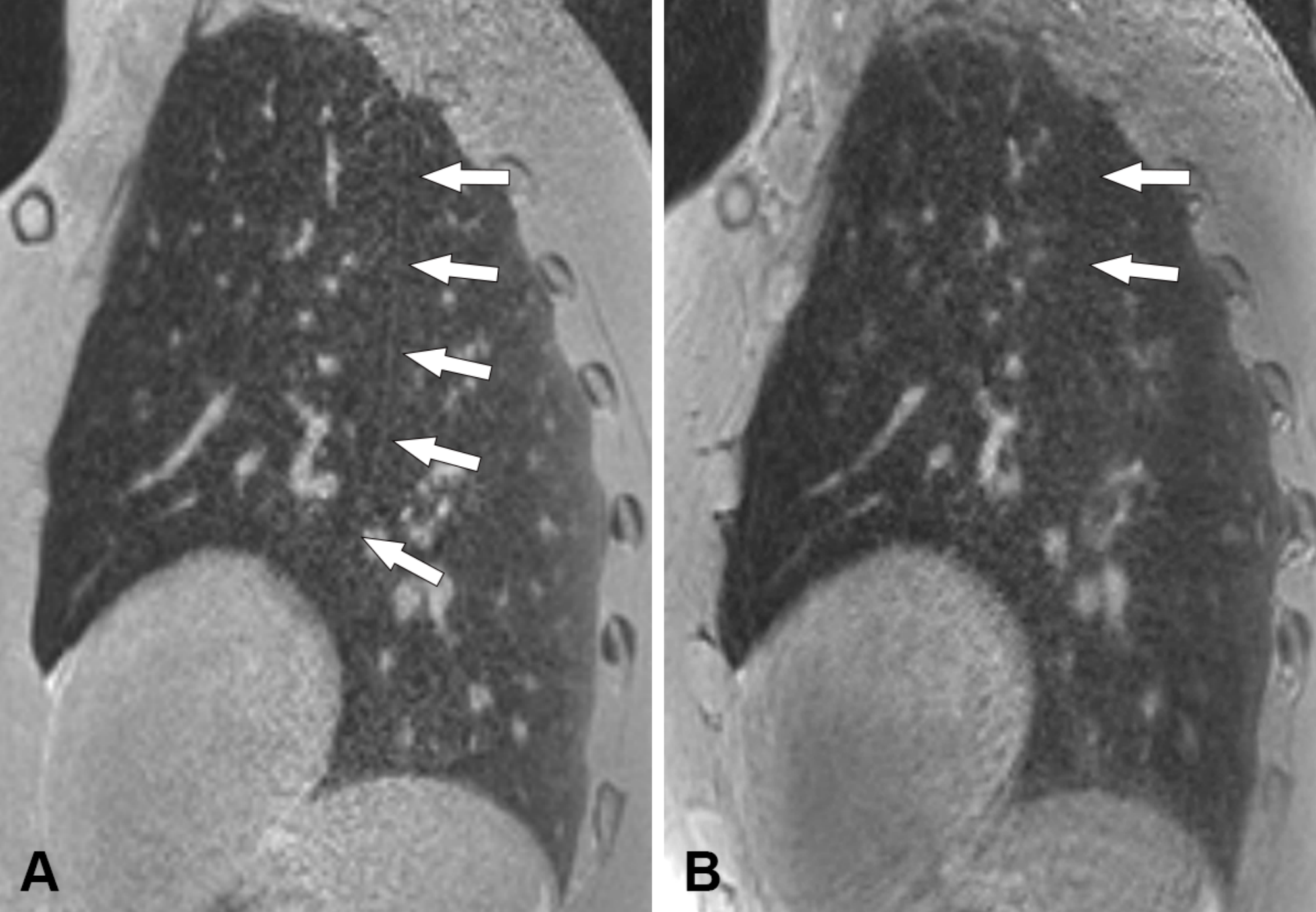
A
B

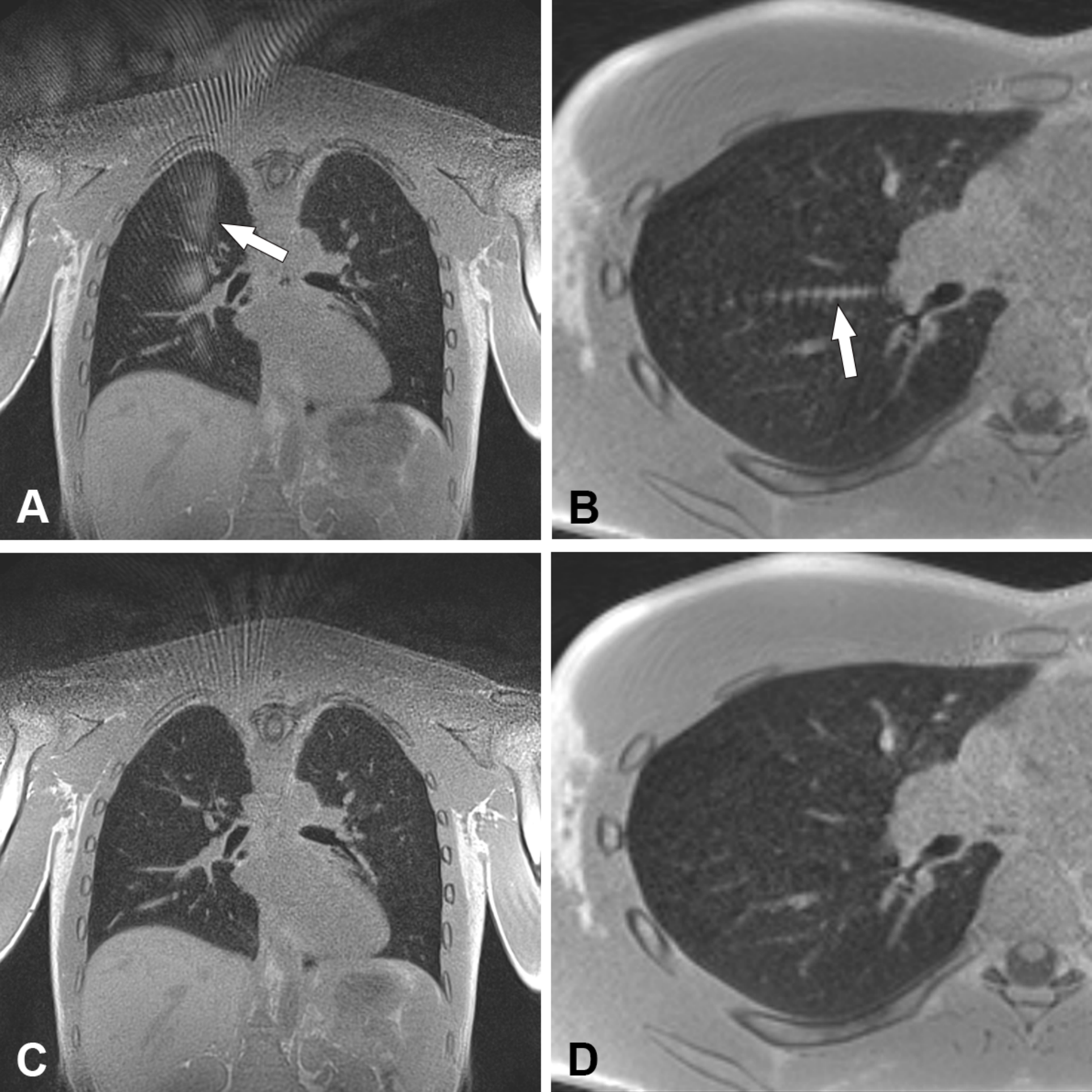
A
B
C
D